

# Experimental demonstration of measurement-based quantum computation in correlation space

Wei-Bo Gao<sup>\*,1</sup>, Xing-Can Yao<sup>\*,1</sup>, Jian-Ming Cai<sup>2,3</sup>, He Lu<sup>1</sup>, Ping Xu<sup>1</sup>,  
Tao Yang<sup>1</sup>, Yu-Ao Chen<sup>1</sup>, Zeng-Bing Chen<sup>1</sup> and Jian-Wei Pan<sup>1,4</sup>

<sup>1</sup>*Hefei National Laboratory for Physical Sciences at Microscale and Department of Modern Physics, University of Science and Technology of China, Hefei, Anhui 230026, China*

<sup>2</sup>*Institut für Quantenoptik und Quanteninformation,*

*Österreichische Akademie der Wissenschaften, Technikerstraße 21A, A-6020 Innsbruck, Austria*

<sup>3</sup>*Institut für theoretische Physik, Universität Innsbruck, Technikerstraße 25, A-6020 Innsbruck, Austria*

<sup>4</sup>*Physikalisches Institut, Ruprecht-Karls-Universität Heidelberg, Philosophenweg 12, 69120 Heidelberg, Germany*

(Dated: December 5, 2018)

The paradigm of measurement-based quantum computation opens new experimental avenues to realize a quantum computer and deepens the understanding of quantum physics [1–3]. For years, the entanglement properties of cluster states have been considered critical for universal measurement-based quantum computation [1–9]. Surprisingly, a novel framework namely quantum computation in correlation space [10–12] has opened new routes to construct quantum states possessing entanglement properties different from cluster states while still retaining the universality for measurement-based quantum computing. The scheme not only offers more flexibility to prepare universal resources for quantum computation, but also provides a different perspective to study the fundamental problem regarding what are the essential features responsible for the speedup of quantum computers over classical devices [13–16]. Here we report an experimental realization of every building block of the model of measurement-based quantum computation in correlation space. In the experiment, we prepare a four-qubit and a six-qubit state, which are proved different from cluster states through two-point correlation functions and the single site entropy of the qubits. With such resources, we have demonstrated a universal set of single-qubit rotations, two-qubit entangling gates and further Deutsch’s algorithm. Besides being of fundamental interest, our experiment proves in-principle the feasibility of universal measurement-based quantum computation without cluster states, which represents a new approach towards the realization of a quantum computer.

Measurement-based quantum computation (MQC) with cluster states, also called one-way quantum computation, has generated enormous interest in the quantum information community since its discovery in 2001 [1–3]. In this computational model, two steps are required (i) preparing an algorithm-independent universal resource state and (ii) performing single-qubit measurements with classical feed-forward of their outcomes. Cluster states [2] have been the only known universal resources for years and so far all the reported experimental demonstration of one-way quantum computation has been based on cluster states [4–8]. Surprisingly, it was found recently by Gross and Eisert that, in the framework of MQC in correlation space many singular entanglement properties of cluster states can be relaxed for a universal resource [10–12].

The discovery has greatly enriched the resources for the implementation of MQC and provided a different perspective to study the fundamental problem, that is, what are the essential features of quantum states responsible for the speedup of quantum computers over classical devices [13–16]? In MQC, the computational power is embedded in the universal resource states, entanglement properties of which can thus provide insights into the essential role of entanglement in the speedup of quantum computation. Entanglement properties of cluster states are usually regarded as being paramount and favorable for quantum computation. For example, in cluster states,

two generic qubits are uncorrelated [9], which makes it possible to logically break down a large scale MQC into small components, and every particle is maximally entangled with the rest of the state in order to guarantee deterministic operations. Nevertheless, in contrast to cluster states, universal resource states with arbitrarily small local entanglement do exist, and a non-vanishing correlation length as a matter of fact is not an obstacle for universal MQC [10–12]. These striking facts offer more flexibility to tailor universal resource states for various kinds of physical systems, e.g. cold atoms and polar molecules in optical lattices [17], or even many-body systems in condensed matter physics [18].

Here we report an experimental realization of MQC in correlation space. First, we prepare a 4-photon 4-qubit state entangled with polarized photons and a 4-photon 6-qubit state entangled in both the polarization and spatial modes. We show that they have entanglement properties different from cluster states by measuring the two-point correlation functions and single-site entropy in the states, although they still satisfy the same entanglement criteria for universality [13, 16]. Based on the generated four-qubit states, single qubit rotations together with the working principle of compensating the measurement randomness are demonstrated. Furthermore, a two-qubit entangling gate is implemented based on the six-qubit state. Our experiment shows that quantum states differ-

ent from cluster states can also serve as promising candidates for one-way quantum computation, and fundamentally not all entanglement properties of cluster states are indispensable for quantum computation.

General universal one dimensional (1D) computational wires are expressed as matrix product states (MPS) [19–21]

$$|\Psi\rangle = \sum_{s_i} \langle r|A[|s_n\rangle] \cdots A[|s_1\rangle]|l\rangle |s_1 \cdots s_n\rangle \quad (1)$$

where  $A[|s_i\rangle]$  are single-qubit operators,  $|l\rangle$  and  $|r\rangle$  represent left and right boundary vectors in the so-called correlation space, which is the auxiliary two-dimensional vector space the matrices  $A[|s_i\rangle]$  act on. A local projective measurement on site  $i$  with the outcome  $|\phi_i\rangle$  will induce the action of the operator  $A[|\phi_i\rangle] = \sum_{s_i} \langle \phi_i | s_i \rangle A[|s_i\rangle]$  in the correlation space, which can serve as the initialization, single qubit rotation and readout of a logical qubit [10–12]. Quantum 1D wires can be coupled to form a 2D resource state for the implementation of entangling gates [12].

In our experiment, the technique of spontaneous parametric down-conversion (SPDC) and linear optical elements are used to generate the resource states (see Methods for the details). A four-qubit 1D MPS (see Fig. 1a) encoded on the polarized photons is used to demonstrate single-qubit rotations. Here we take the left and right boundary vectors as  $|l\rangle = |+\rangle$  and  $|r\rangle = |0\rangle$ , where  $|+\rangle = \frac{1}{\sqrt{2}}(|0\rangle + |1\rangle)$ . Moreover, for the first three sites of the state, the tensor matrices are [16]

$$A[|H\rangle] = \hat{H} \cos \theta \quad \text{and} \quad A[|V\rangle] = \hat{H} \hat{Z} \sin \theta. \quad (2)$$

Here  $|H\rangle$  and  $|V\rangle$  denote the horizontal and vertical polarization, which represent the qubits  $|0\rangle$  and  $|1\rangle$ ;  $\hat{H}$  denotes the Hadamard gate and  $\hat{Z}$  refers to the Pauli matrix  $\sigma_z$ . For the end site, we adopt a simple alternative by changing the tensor matrix to  $B[|H\rangle] = \hat{H}$ ,  $B[|V\rangle] = \hat{H} \hat{Z}$ . Substituting them into equation (1), the four-qubit state is explicitly written as

$$|\psi_4\rangle = c|H\rangle_1 (c|H\rangle + s|V\rangle)_2 (c|H\rangle |P\rangle + s|V\rangle |M\rangle)_{34} \\ + s|V\rangle_1 (c|H\rangle - s|V\rangle)_2 (c|H\rangle |M\rangle + s|V\rangle |P\rangle)_{34}, \quad (3)$$

where  $|P\rangle = \frac{1}{\sqrt{2}}(|H\rangle + |V\rangle)$  and  $|M\rangle = \frac{1}{\sqrt{2}}(|H\rangle - |V\rangle)$ . For simplicity, we denote  $c = \cos \theta$  and  $s = \sin \theta$  in the above equation and the following text. For any  $\theta$  that  $\cos \theta \neq 0$  and  $\sin \theta \neq 0$ , such a MPS can serve as a quantum wire for single qubit logic gates [16]. By tuning the parameter  $\theta$ , the entanglement properties can be very different. In our experiment we choose the angle  $\theta$  as  $\pi/6$ , and thus  $c = \sqrt{3}/2$ ;  $s = 1/2$ . In this state, the processing of logical information is implemented in the part of qubits with the tensor matrix  $A$ ; while the last

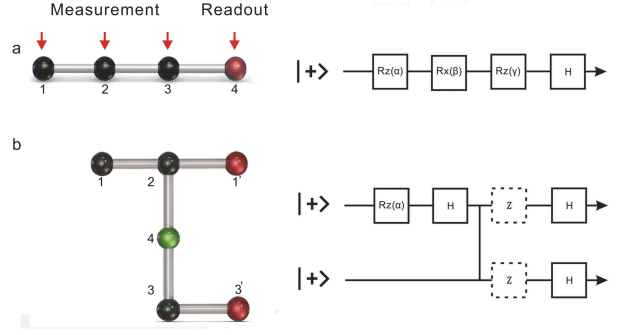


FIG. 1: **a.** A four-qubit state for the implementation of single qubit rotations. The black dots are associated with the tensor matrices  $A[|H\rangle] = \hat{H} \cos \theta$  and  $A[|V\rangle] = \hat{H} \hat{Z} \sin \theta$ , while the red dots are associated with  $B[|H\rangle] = \hat{H}$ ,  $B[|V\rangle] = \hat{H} \hat{Z}$ . The measurements on the first three qubits will implement the quantum circuit on the right. **b.** A six-qubit state for the implementation of a two-qubit entangling gate. The horizontal lines (1-2-1' and 3-3') represent two computational wires corresponding to two logical qubits. To couple them, we prepare site 4 as  $\frac{1}{\sqrt{2}}(|H\rangle + |V\rangle)$  and then apply two controlled-Z operations on qubits 2-4 and 3-4. The measurements on the qubits 1-2-3-4 will implement a C-Phase gate shown on the right. The  $\hat{Z} \otimes \hat{Z}$  operation will depend on the measurement result of qubit 4, and thus they are drawn in dashed squares.

site serves as readout and has the function of mapping the logical information carried by the correlation system to the physical qubit as  $|0\rangle_c \rightarrow |P\rangle_p$  and  $|1\rangle_c \rightarrow |M\rangle_p$  [16].

To demonstrate the two-qubit entangling gate, a 2D resource state is required. As shown in Fig. 1b, our 2D state is constructed by coupling two 1D MPS (1-2-1' and 3-3') with site 4 via a general scheme to construct universal resources from arbitrary computational wires (see Appendix). The coupling is implemented by first preparing site 4 as  $|P\rangle$ , and then applying two controlled-phase operations between qubits 2-4 and 3-4. We use the spatial degree of freedom  $|H'\rangle$  and  $|V'\rangle$  of photons to carry the qubits 1' and 3'. The corresponding tensor matrices are respectively  $B[|H'\rangle_{1'}] = B[|P'\rangle_{3'}] = \hat{H}$ ,  $B[|V'\rangle_{1'}] = B[|M'\rangle_{3'}] = \hat{H} \hat{Z}$  with  $|P'\rangle = \frac{1}{\sqrt{2}}(|H'\rangle + |V'\rangle)$  and  $|M'\rangle = \frac{1}{\sqrt{2}}(|H'\rangle - |V'\rangle)$ . The four-photon six-qubit state is thus as follows

$$|\psi_6\rangle = |H\rangle_4 |\mu\rangle_{121'} |\nu\rangle_{33'} + |V\rangle_4 \hat{Z}_2 |\mu\rangle_{121'} \hat{Z}_3 |\nu\rangle_{33'} \quad (4)$$

where

$$|\mu\rangle = c^2|HHH'\rangle + cs|HVVH'\rangle + cs|VHVV'\rangle - s^2|VVVV'\rangle, \\ |\nu\rangle = \frac{1}{2}(c|HHH'\rangle + s|VVV'\rangle), \quad (5)$$

and  $\hat{Z}_i$  represents the Pauli matrix  $\sigma_z$  applied on qubit  $i$ .

For the four-qubit state, we have obtained  $F = \langle \psi_4 | \rho | \psi_4 \rangle = 0.74 \pm 0.01$  by estimating the density matrix of the experimental state. For the six-qubit state,

we have also calculated its fidelity  $F = \langle \psi_6 | \rho | \psi_6 \rangle = 0.73 \pm 0.01$  by measuring 36 measurement settings in the local decomposition of  $|\psi_6\rangle\langle\psi_6|$  (see Appendix for the details).

Furthermore, we verify that the entanglement properties of our resource states are much different from cluster states by measuring both two-point correlations and local entanglement. The two-point correlation between qubit  $i$  and  $j$  is defined as  $\mathcal{Q}_{ab}^{ij}(|\Psi\rangle) = \langle \Psi | \hat{a}_i \otimes \hat{b}_j | \Psi \rangle - \langle \Psi | \hat{a}_i | \Psi \rangle \langle \Psi | \hat{b}_j | \Psi \rangle$ , where  $\hat{a}_i$  and  $\hat{b}_j$  are respectively Pauli matrices acting on qubits  $i$  and  $j$ . In the state  $|\psi_4\rangle$ , there is non-zero two-point correlation, i.e.  $\mathcal{Q}_{XX}^{13} = 0.375$ , while the corresponding one in the cluster state is zero [9], namely  $\mathcal{Q}_{max}^{13} = \max_{a,b=X,Y,Z} |\mathcal{Q}_{ab}^{13}| = 0$ . Similarly, in the six-qubit state  $|\psi_6\rangle$ , we have theoretical values  $\mathcal{Q}_{XX}^{24} = 0.433$ ,  $\mathcal{Q}_{ZX}^{34} = 0.375$ . While for the corresponding cluster state, the two-point correlations  $\mathcal{Q}_{max}^{24}$  and  $\mathcal{Q}_{max}^{34}$  are zero [9]. Experimentally, we find  $\mathcal{Q}_{xx}^{13} = 0.26 \pm 0.01$  for  $|\psi_4\rangle$ ; and  $\mathcal{Q}_{xz}^{24} = 0.41 \pm 0.02$ ,  $\mathcal{Q}_{zx}^{34} = 0.32 \pm 0.02$  for  $|\psi_6\rangle$ . Although the experimental data is not ideal, none of the tested two-point correlations equals zero, clearly showing that our states are not cluster states.

Local entanglement between one single qubit  $i$  and the other qubits is quantified by the local entropy  $E(\rho_i) = 2(1 - \text{Tr}\rho_i^2)$ , where  $\rho_i$  is the reduced density matrix of qubit  $i$  [22]. In a cluster state, every qubit is maximally entangled with the rest of the state, and thus the local entropy always equals 1 [2, 9]. Instead, in the resource state  $|\psi_4\rangle$ , we have theoretically  $E(\rho_1) = E(\rho_3) = 0.75$  and  $E(\rho_2) = 0.5625$ . In  $|\psi_6\rangle$ ,  $E(\rho_1) = E(\rho_2) = E(\rho_3) = 0.75$  and  $E(\rho_4) = 0.9375$ . Experimentally, in  $|\psi_4\rangle$ , the local entropy are respectively  $E(\rho_1) = 0.93 \pm 0.01$ ;  $E(\rho_2) = 0.63 \pm 0.01$ ;  $E(\rho_3) = 0.88 \pm 0.01$ . In  $|\psi_6\rangle$ ,  $E(\rho_1) = 0.62 \pm 0.02$ ;  $E(\rho_2) = 0.80 \pm 0.02$ ;  $E(\rho_3) = 0.67 \pm 0.02$ ;  $E(\rho_4) = 0.90 \pm 0.02$ . The experimental data is imperfect; however, none of them are equal to 1, which shows the different entanglement properties of our resource states from the cluster states.

To realize an arbitrary  $SU(2)$  single-qubit rotation, we measure the qubits of the four-qubit state  $|\psi_4\rangle$  in the basis  $B(\zeta) = \{|\zeta_0\rangle, |\zeta_1\rangle\}$ , where  $|\zeta_0\rangle = s|H\rangle + ic \tan \frac{\zeta}{2} |V\rangle$  and  $|\zeta_1\rangle = c|H\rangle - is \cot \frac{\zeta}{2} |V\rangle$ . For simplicity, we define the outcome  $r_j$  to be 0 if the measurement result is  $|\zeta_0\rangle$ , and as 1 if the result is  $|\zeta_1\rangle$ . We first consider the case when all the measurement outcomes are 0. This will reduce the success probability of the gate for each step of measurement, but it suffices as a proof-of-principle to demonstrate the single-qubit gate (the strategy to compensate the wrong outcome and improve the success probability will be demonstrated in the following text). In each measurement step, single qubit rotation  $R_z(\zeta) = \exp(-i\zeta\sigma_z/2)$ , followed by a Hadamard operation, can be implemented. Based on the generated four-qubit state, we perform consecutive measurements  $B_1(\alpha)$ ,  $B_2(\beta)$ ,  $B_3(\gamma)$  on the physical qubits

1, 2, 3. By doing so, the input state of the correlation system  $|\psi_{in}\rangle_c = |+\rangle$  is transformed into  $|\psi_{out}\rangle_c = \hat{H}R_z(\gamma)R_x(\beta)R_z(\alpha)|+\rangle$ , where  $R_x(\beta) = \exp(-i\beta\sigma_x/2)$  (See Fig. 1a). Following the map induced by the tensor matrix  $B$ , the output state of the physical state is  $|\psi_{out}\rangle_p = R_z(\gamma)R_x(\beta)R_z(\alpha)|+\rangle_{|0\rangle \rightarrow H,1\rangle \rightarrow V}$ . The experimental fidelities of six states are shown in Table. I., the average of which is  $0.86 \pm 0.01$ , clearly above the classical threshold  $2/3$  [23]. More results of the single-qubit gate can be found in the Appendix.

$\alpha$	$\beta$	$\gamma$	$ \psi_{out}\rangle_c$	$ \psi_{out}\rangle_p$	fidelity
0	0	0	$ 0\rangle$	$ P\rangle$	$0.92 \pm 0.01$
$\pi$	$\pi$	0	$ 1\rangle$	$ M\rangle$	$0.72 \pm 0.02$
$\pi/2$	$\pi/2$	$\pi/2$	$ +\rangle$	$ H\rangle$	$0.80 \pm 0.02$
$-\pi/2$	$\pi/2$	$\pi/2$	$ -\rangle$	$ V\rangle$	$0.91 \pm 0.01$
$\pi$	$\pi$	$\pi/2$	$ I_0\rangle$	$ L\rangle$	$0.93 \pm 0.01$
$\pi$	$\pi$	$-\pi/2$	$ I_1\rangle$	$ R\rangle$	$0.86 \pm 0.02$

TABLE I: The fidelities of the output states of the single-qubit rotation. The first three qubits of the four-qubit cluster state are measured in basis  $B(\alpha)$ ,  $B(\beta)$ ,  $B(\gamma)$ .  $|\psi_{out}\rangle_c$  and  $|\psi_{out}\rangle_p$  represent the output states in the correlation space and the physical world, respectively.  $|I_0\rangle = \frac{1}{\sqrt{2}}(|0\rangle + i|1\rangle)$ , and  $|I_1\rangle = \frac{1}{\sqrt{2}}(|0\rangle - i|1\rangle)$ .

A distinct feature of MQC in correlation space is the strategy to compensate the randomness of measurement outcome. In cluster state quantum computation, the wrong measurement outcome only induces by-product Pauli operators, which can be compensated by using feed-forward control of future measurement basis. The by-product operators in MQC in correlation space can be different from Pauli matrices, and the simple feed-forward technique does not work in general any more. Fortunately, it has been proved that the introduced errors can still be efficiently corrected in a bounded number of steps with the trial-until-success strategy [10–12].

As a proof-of-principle, we compare the success probability of implementing the rotation  $\hat{H}R_z(\alpha)|+\rangle$  with a two-qubit state  $|\lambda_{34}\rangle = c|H\rangle_3|P\rangle_4 + s|V\rangle_3|M\rangle_4$  and with the four-qubit state  $|\psi_4\rangle$ . Based on the two-qubit state, we measure qubit 1 in the basis  $B(\alpha)$ . When the outcome  $r_1 = 0$ , we obtain the desired single-qubit rotation  $\hat{H}R_z(\alpha)|+\rangle$  with a success probability  $p_s(\alpha)$ . However, when  $r_1 = 1$ , we obtain a rotation  $\hat{H}R_z(\alpha')|+\rangle$  but with a wrong angle  $\tan(\alpha'/2) = (-1/3) * \cot(\alpha/2)$ . Based on the four-qubit state, we first measure qubit 1 in the basis  $B(\alpha)$ . When obtaining  $r_1 = 0$ , we measure the qubits 2 and 3 in the  $Z$  basis, resulting an output state  $\hat{X}^{r_3}\hat{Z}^{r_2}\hat{H}R_z(\alpha)|+\rangle$ . When  $r_1 = 1$ , we measure the second qubit in the  $Z$  basis with the outcome  $r_2$  and the third qubit in the basis  $B[(-1)^{r_2}(\alpha - \alpha')]$ . When  $r_3 = 0$ , with a probability  $p_s(\alpha - \alpha')$ , we obtain the output state  $\hat{Z}^{r_2}\hat{H}R_z(\alpha)|+\rangle$ . The final result

is equivalent to the desired rotation up to a Pauli by-product operator. Thus, with two more qubits, we can boost the success probability of the rotation from  $p_s(\alpha)$  to  $p_s(\alpha) + [1 - p_s(\alpha)] \cdot p_s(\alpha - \alpha')$  (See Appendix for the case of more qubits).

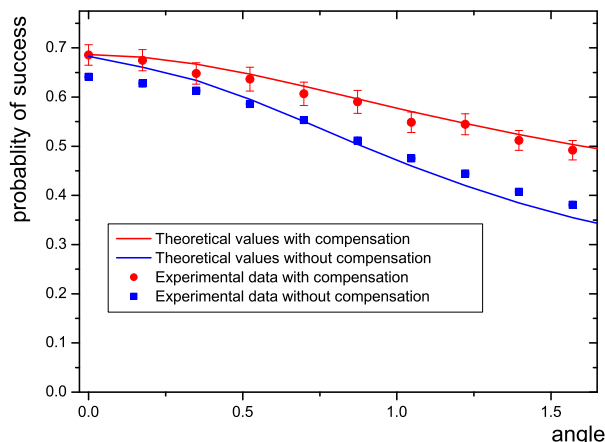


FIG. 2: Theoretical and experimental success probability of compensating the rotation error with two-qubit states and four-qubit states. The blue (red) lines represent the theoretical success probability under the white noise model in the two-qubit (four-qubit) case. The blue (red) dots represent the experimental values in the two-qubit (four-qubit) case, which are achieved by measuring the states for 5s (300s). From the figure, we can see that the success probability has been enhanced by using two more qubits. The experimental data is in good agreement with the theoretical values when considering the effects of white noise.

The experimental success probability in the four-qubit case is achieved by measuring in the appropriate basis and then adding the probability of each successful measurement branch. In the analysis of the experimental data, we calculate the corresponding theoretical success probability with the states under the white noise model. In other words, we write the two states as:

$$\begin{aligned} \rho_2 &= p|\lambda_{34}\rangle\langle\lambda_{34}| + (1-p)\frac{I_2}{4}, \\ \rho_4 &= p'|\psi_4\rangle\langle\psi_4| + (1-p')\frac{I_4}{16}, \end{aligned} \quad (6)$$

where  $I_2(I_4)$  denotes two-qubit (four-qubit) identity matrix;  $p = (4f_2 - 1)/3$ ;  $p' = (16f_4 - 1)/15$  and  $f_2(f_4)$  is the fidelity of the two-qubit (four-qubit) state, that is, 0.90 (0.73). The theoretical and experimental success probabilities are shown in Fig. 2, from which we can see that, the experimental data is well consistent with the theoretical curve and the success probability has indeed been increased with compensation.

Besides single-qubit rotations, a two-qubit entangling

gate is required to demonstrate universal quantum computing. Based on the six-qubit state  $|\psi_6\rangle$ , we have realized a two-qubit controlled phase gate. We first measure qubit 1 in the basis  $B(\alpha)$ . When  $r_1 = 0$  (we only consider this case in the following text, the other outcome just corresponds to a different input), this measurement initializes the input state of the correlation system as  $\hat{H}R_z(\alpha)|+\rangle_t \otimes |+\rangle_c$ , where  $t$  and  $c$  denote the target and control logical qubit corresponding to two computational wires (1-2-1' and 3-3'). Then, we measure qubit 2 and 3 in the basis  $B(\frac{\pi}{2}) = \{s|H\rangle + ic|V\rangle, c|H\rangle - is|V\rangle\}$ . (a) Once having the outcome  $r_2 = r_3 = 0$ , we measure qubit 4 in the Y basis  $\{|H\rangle + i|V\rangle, |H\rangle - i|V\rangle\}$  and transform the logical state carried by the correlation systems from  $|\psi_{in}\rangle = \hat{H}R_z(\alpha)|+\rangle_t \otimes |+\rangle_c$  to  $|\psi_{out}\rangle = (\hat{H} \otimes \hat{H}) \cdot (\hat{Z} \otimes \hat{Z})^{r_4} \cdot CZ|\psi_{in}\rangle$ , where  $CZ = I \otimes |0\rangle\langle 0| + \hat{Z} \otimes |1\rangle\langle 1|$  is the controlled phase gate. The tensor matrices corresponding to qubits 1' and 3' map the logical output state to the physical output state [16] carried by qubits 1' and 3' as  $(I \otimes \hat{H}) \cdot (\hat{Z}_{1'} \otimes \hat{Z}_{3'})^{r_4} \cdot (|0\rangle|+\rangle - i \tan \frac{\alpha}{2}|1\rangle|-\rangle)_{1'3'}|_{0 \rightarrow H', 1 \rightarrow V'}$ . (b) If  $r_2 \neq 0$  or  $r_3 \neq 0$ , we measure qubit 4 in the Z basis and decouple two 1D wires. After the measurement, a local rotation error will appear on each logical qubit. The same as in the single-qubit gate, we can efficiently correct them by applying the trial-until-success strategy if we have more qubits.

In the experiment, when  $r_2 = r_3 = 0$ , we characterize the output state of the two-qubit gate by the method of state tomography. We collect the experimental data for 600s for each of 36 combinations of the measurement basis  $\{|H'\rangle, |V'\rangle, |P'\rangle, |M'\rangle, |R'\rangle, |L'\rangle\}$ , where  $|R'\rangle = \frac{1}{\sqrt{2}}(|H'\rangle + i|V'\rangle)$  and  $|L'\rangle = \frac{1}{\sqrt{2}}(|H'\rangle - i|V'\rangle)$ , and then estimate the density matrix with the maximum likelihood technique. The theoretical and experimental density matrices of physical output states when  $\alpha = 0, r_4 = 0$  and  $\alpha = \pi/3, r_4 = 0$  are shown in Fig. 3. The states are in good agreement with the ideal states, which can be seen from their fidelities:  $0.88 \pm 0.02$  and  $0.84 \pm 0.03$ .

When  $r_2 \neq 0$  or  $r_3 \neq 0$ , we have measured the fidelity between the experimental states and the expected ones. In the experiment,  $\alpha$  is fixed as one of the angles of  $0, \pi/2, \pi, \pi/3, -\pi/3$ . When  $r_2 = 0, r_3 = 1$ , the average fidelity of the measured output states is  $0.88 \pm 0.01$ ; when  $r_2 = 1, r_3 = 0$ , the average fidelity is  $0.85 \pm 0.01$ ; when  $r_2 = 1, r_3 = 1$ , the average fidelity is  $0.87 \pm 0.01$ . The results are well consistent with the theoretical predictions. More data when  $r_2 = r_3 = 0$  and the detailed fidelities when  $r_2 \neq 0$  or  $r_3 \neq 0$  are shown in the Appendix.

The realization of multiqubit quantum algorithms is the ultimate goal of quantum computation and the experimental community has made considerable efforts toward this aim. Deutsch's algorithm represents an interesting instance of demonstrating the power of quantum computation over classical computation. It has been experimentally reported in the quantum circuit model [24] and the

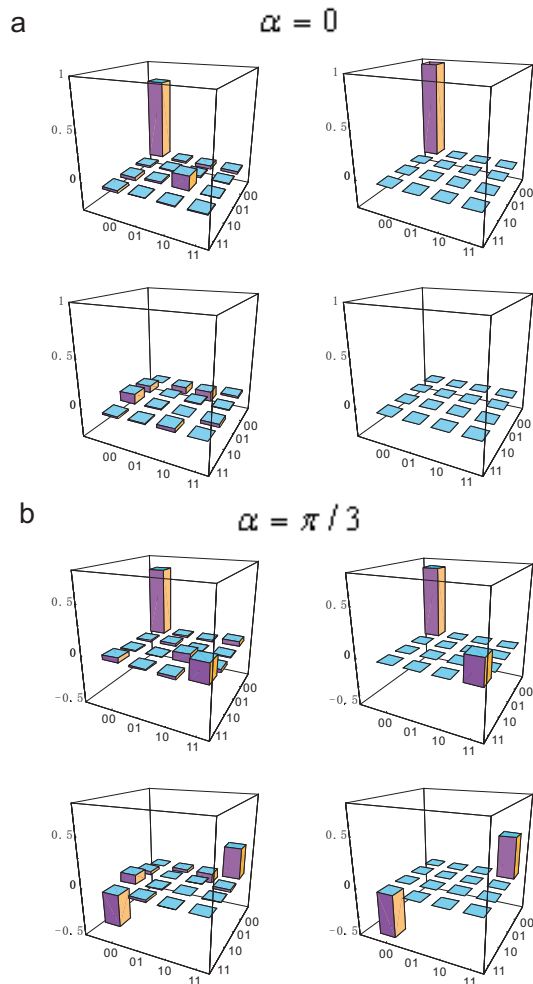


FIG. 3: The density matrices of the output states of the entangling two-qubit gate. The left column shows the real and the imaginary part of the experimental output state density matrices, while the right column shows the theoretical density matrices. In cases **a** and **b**, qubit 1 is respectively measured in bases  $B(0)$  and  $B(\pi/3)$ . All the matrices are achieved in the case when the outcome of the measurements is  $r_1 = r_2 = r_3 = r_4 = 0$ .

one-way computation model based on cluster states [25]. Here we experimentally demonstrate the implementation of Deutsch's algorithm based on the six-qubit states  $|\psi_6\rangle$ .

Deutsch's algorithm, also known as the Deutsch-Jozsa algorithm [26], allows one to distinguish two different types of function  $f(x)$  implemented by an oracle in a black box. The function  $f(x)$  with an  $N$ -bit binary input  $x$  is constant if it returns the same value (either 0 or 1) for all possible inputs and balanced if it returns 0 for half of the inputs and 1 for the other half. With classical methods, in some cases we have to query this oracle as many as  $2^{N-1} + 1$  times. However, only one query is required in all cases by using quantum computation [26]. In the two-qubit version, the applied algorithm can be demonstrated as  $|x\rangle|y\rangle \rightarrow |x\rangle|y \oplus f(x)\rangle$ , where

$|x\rangle$  is the query input qubit and  $|y\rangle$  is the ancilla input qubit. Preparing  $|x\rangle|y\rangle$  as  $|+\rangle|-\rangle$ , we can get the output states  $[(-1)^{f(0)}|0\rangle + (-1)^{f(1)}|1\rangle]|-\rangle$ . Finally, we apply two Hadamard operations on the two output qubits. If  $f(x)$  is constant, the final result will be  $|H\rangle|V\rangle$ , while if it is balanced, the final result will be  $|V\rangle|V\rangle$ . Therefore, now we can determine the types of  $f(x)$  from the output states. There are two types of constant function, namely  $f_1 = I \otimes I$  and  $f_2 = I \otimes \sigma_x$ . Also, there are two types of balanced function, namely  $f_3 = g_{cnot}$  and  $f_4 = g_{cnot}(I \otimes \sigma_x)$ , where  $g_{cnot}$  represents a controlled-not gate. Since  $f_2$  and  $f_4$  can be achieved from  $f_1$  and  $f_3$  by single-qubit local operation, in the following we consider only the functions  $f_1$  and  $f_3$ .

In the experiment, we use the wire 3-3' of  $|\psi_6\rangle$  to carry the query logical qubit and 1-2-1' of  $|\psi_6\rangle$  for the ancilla logical qubit. In the following, we consider the implementation of Deutsch's algorithm when  $r_1 = r_2 = r_3 = r_4 = 0$ . The measurement of qubit 1 in the basis  $B(\pi)$  and qubits 2, 3, 4 in the basis  $B(0)$  performs the transformation  $H_q \otimes R_z(\pi)_a$ . Moreover, considering the map of logical qubits from correlation systems into the physical qubits the final transformation of the inputs will be  $(\hat{H}_q \otimes \hat{H}_a)(I_q \otimes R_z(\pi)_a)$ , which implements the preparation of ancilla qubit  $|-\rangle$ , the constant function and the readout of the qubits (See Fig. 4a). Similarly, by measuring qubit 1 in the basis  $B(\pi/2)$  and qubits 2, 3, 4 in the basis  $B(\pi/2)$ , we can implement the gate  $(H_q \otimes H_a)g_{cnot}(I_q \otimes R_z(\pi)_a)$  on the inputs, which is the case when the function is balanced (See Fig. 4b). Here the measurement of qubits 2, 3 and 4, together with the detector signal corresponding to  $r_1 = r_2 = r_3 = r_4 = 0$  should be viewed as the entire black box. In the experiment, the success probability of recognizing the type of  $f(x)$  is as large as  $99\% \pm 1\%$  for  $f_1$  and  $75\% \pm 2\%$  for  $f_3$ . The non-ideal probability is mainly caused by the non-perfect resource state and single-photon interferometers in the setup. In the Appendix, we have discussed in detail the cases when some measurement outcomes are not 0.

In summary, we have realized a proof-of-principle experimental demonstration of measurement-based quantum computation in correlation space. Every building block of the scheme and a simple yet interesting algorithm has been demonstrated, providing evidence of promising applications of states different from cluster states. These new resource states do not possess many apparently necessary entanglement properties of cluster states, such as vanishing correlation functions and being locally maximally mixed, but nevertheless are universal for quantum computation.

There are many open questions, both theoretical and experimental, worth investigating in the future. In measurement-based quantum computation with cluster states, it is known that if the product of the number resolving detector efficiency and the source efficiency is

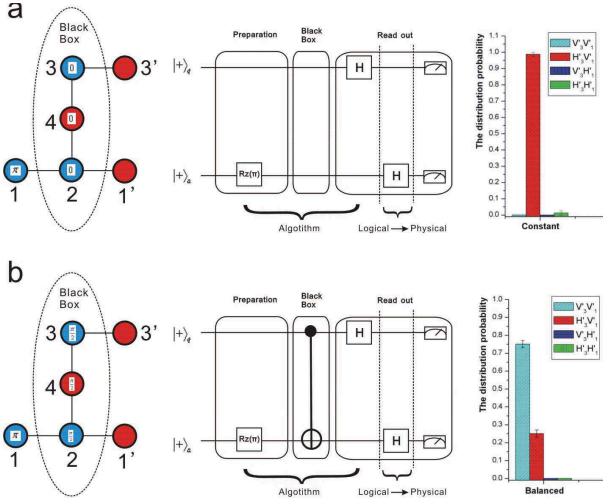


FIG. 4: The theoretical design and the experimental results of implementing Deutsch's algorithm. The wire 3-3' represents the query logical qubit, and the wire 1-2-1' represents the ancilla logical qubit. In **a** and **b**, the measurement patterns on the physical qubits (left) implement the algorithm on the logical qubits (right). The angles  $\alpha$  represent the measurement basis  $B(\alpha)$  of each physical qubit. In the circuit, the operation  $(I \otimes \hat{H})$  represents the mapping of the qubits from the correlation space to the realistic physical world. The final results are carried by the qubits 3' and 1'. The success probability of recognizing the constant function is  $99\% \pm 1\%$ , while for the balanced function, this probability is  $75\% \pm 2\%$ .

greater than  $2/3$ , efficient linear optical quantum computation is possible [27]. With novel resource states for quantum computation in correlation space, computation will probably require more qubits. However, bonds between two particles are easier to create the lower the required entanglement [28]. It would be interesting to investigate what conditions are required to make the latter scheme scalable. For realistic systems, a trade-off may exist between the effort of preparing a universal resource and its efficiency for quantum computation. The feed-forward rule also warrants further study, and it would be desirable to combine the feed-forward technique with the proof-of-principle demonstration.

## METHOD

### Creation of the resource states.

In our experiment, entangled photons are created by using type-II parametric down conversion [29]. Femtosecond laser pulses ( $\approx 200$  fs, 76 MHz, 788nm) are converted to ultraviolet pulses through a frequency doubler  $LiB_3O_5$  (LBO) crystal and the ultraviolet laser pulse passes through two nonlinear crystals (BBO), generating two pairs of photons in path 1-2 and 3-4. The observed two-fold coincident count rate is about  $5.4 \times 10^4/s$ .

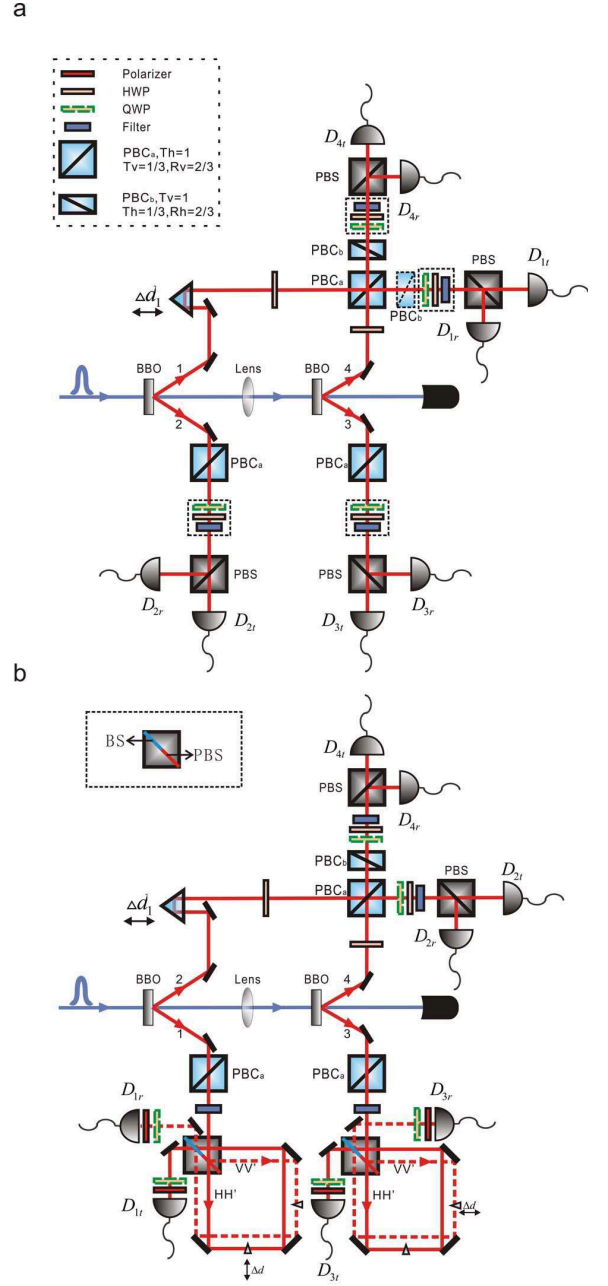


FIG. 5: Experimental setup for (a) the generation of the four-qubit state  $|\psi_4\rangle$  and (b) the six-qubit state  $|\psi_6\rangle$ . **a.** An ultraviolet pulse passes through two BBO crystals to create two pairs of entangled photons. Then, half-wave plates (HWP) and a series of polarization dependent beam splitter cubes (PBCs) have been used to create the desired state. Prism  $\Delta d_1$  is used to ensure that the input photons arrive at the PBCs at the same time. Furthermore, every output is spectrally filtered ( $\Delta\lambda_{FWHM} = 3.2$  nm) to ensure good temporal overlap. A combination of HWP, quarter-wave plates (QWP) and polarization beam splitter (PBS) has been used to implement the measurement setups. **b.** By exchanging the labels of 1 and 2 of  $|\psi_4\rangle$ , and letting the photons 1 and 3 enter two PBSs, the desired six-qubit state  $|\psi_6\rangle$  can be prepared. The ultra-stable Sagnac-ring interferometers have been used to measure the spatial qubits. In the interferometer, the specially designed beam-splitter cubes are half PBS-coated and half beam splitter coated and high-precision small-angle prisms are used to satisfy fine adjustments of the relatively delay of the two different paths.

First, let's consider the preparation of the four-qubit cluster state. By placing half-wave plates, we prepare the initial two-photon states as

$$1/\sqrt{2}(|H\rangle_1|P\rangle_2 + |V\rangle_1|M\rangle_2) \quad (7)$$

and

$$1/\sqrt{2}(|H\rangle_3|P\rangle_4 + |V\rangle_3|M\rangle_4). \quad (8)$$

Then, two polarization dependent beam splitter cubes ( $PBC_a$ ) with  $T_v = (s/c)^2$  and  $T_h = 1$  are placed in paths 2 and 3, where  $T_v$  ( $T_h$ ) represents the transmission probability for the vertical (horizontal) polarization. This will transform the entangled two-qubit states into

$$1/\sqrt{2}(|H\rangle_1(c|H\rangle + s|V\rangle)_2 + |V\rangle_1(c|H\rangle - s|V\rangle)_2) \quad (9)$$

and

$$1/\sqrt{2}(c|H\rangle_3|P\rangle_4 + s|V\rangle_3|M\rangle_4). \quad (10)$$

Finally, we let photons 1 and 4 enter a series of PBCs. According to the method in Ref. [30], we can apply a C-phase gate between qubit 1 and 4 through a combination of PBCs, which includes an overlapping  $PBC_a$  ( $T_v = 1/3$  and  $T_h = 1$ ), and a  $PBC_b$  ( $T_v = 1$  and  $T_h = 1/3$ ) in each path of 1 and 4. Note that the function of  $PBC_b$  in path 1 is only to adjust the amplitude of  $|H\rangle_1$  and  $|V\rangle_1$ . Therefore, by removing the  $PBC_b$  in path 1 (using only the overlapping  $PBC_a$ , the  $PBC_b$  in path 4), we can prepare exactly the state  $|\psi_4\rangle$ .

Next, let's consider the preparation of the six-qubit state  $|\psi_6\rangle$ . Based on the created state  $|\psi_4\rangle$ , we exchange the labels of the outputs 1 and 2. Then, we let each of the photons 1 and 3 enter a PBS (see Fig. 5b). Since a PBS transmits  $H$  and reflects  $V$  polarization,  $H$ -polarized photons will follow one path and  $V$ -polarized photons will follow the other. In this way, two spatial qubits are added onto the polarization qubits 1 and 3:  $|H\rangle_i \rightarrow |HH'\rangle_{i,i'}$  and  $|V\rangle_i \rightarrow |VV'\rangle_{i,i'}$ , where  $i = 1, 3$  and the levels are denoted as  $|H'\rangle$  for the first path and  $|V'\rangle$  for the latter path. After these operations, the final state is converted to exactly  $|\psi_6\rangle$ , a four-photon six-qubit non-cluster state. In the experiment, the spatial qubits play the role of reading out the results, and we need to measure the spatial qubits in the  $X, Y$  bases, which requires matching different spatial modes on a common BS. We have designed a special crystal combining a PBS and a beam splitter, and then we have used Sagnac-ring interferometers to construct the required single-photon interferometers, which can be stable for almost 10 hours [31].

We thank H. J. Briegel for valuable suggestions, and J. Eisert for helpful discussions. This work is supported by the NNSF of China, the CAS, the National Fundamental Research Program (under Grant No. 2006CB921900),

the Fundamental Research Funds for the Central Universities. The research at Innsbruck is supported by the FWF (J.-M. C. through the Lise Meitner Program, SFB-FoQuS) and the European Union (QICS, SCALA).

\* These authors contributed equally to this work.

- 
- [1] R. Raussendorf and H. J. Briegel, *Phys. Rev. Lett.* **86**, 5188–5191 (2001).
  - [2] H. J. Briegel and R. Raussendorf, *Phys. Rev. Lett.* **86**, 910–913 (2001).
  - [3] H. J. Briegel et al., *Nature Physics* **51**, 19-26 (2009).
  - [4] P. Walther et al., *Nature (London)* **434**, 169 (2005);
  - [5] N. Kiesel et al., *Phys. Rev. Lett.* **95**, 210502 (2005).
  - [6] C. Y. Lu et al., *Nature Physics* **3**, 91 (2007).
  - [7] Y. Tokunaga et al., *Phys. Rev. Lett.* **100**, 210501 (2008).
  - [8] G. Vallone et al., *Phys. Rev. Lett.* **100**, 160502 (2008).
  - [9] M. Hein et al., In *Proceedings of the International School of Physics “Enrico Fermi” on “Quantum Computers, Algorithms and Chaos”* IOS Press, Amsterdam (2006).
  - [10] D. Gross and J. Eisert, *Phys. Rev. Lett.* **98**, 220503 (2007).
  - [11] D. Gross et al., *Phys. Rev. A* **76**, 052315 (2007).
  - [12] D. Gross and J. Eisert, arXiv:quant-ph/0810.2542.
  - [13] M. Van den Nest et al., *Phys. Rev. Lett.* **97**, 150504 (2006);
  - [14] D. Gross, S. T. Flammia, J. Eisert, *Phys. Rev. Lett.* **102**, 190501 (2009).
  - [15] M. Bremner, C. Mora, and A. Winter, *Phys. Rev. Lett.* **102**, 190502 (2009).
  - [16] J.-M. Cai, W. Dür, M. Van den Nest, A. Miyake, and H. J. Briegel, *Phys. Rev. Lett.* **103**, 050503 (2009).
  - [17] B. Vaucher, A. Nunnenkamp, and D. Jaksch, *New J. Phys.* **10**, 023005 (2008).
  - [18] G. K. Brennen, A. Miyake, *Phys. Rev. Lett.* **101**, 010502 (2008).
  - [19] M. Fannes, B. Nachtergaele, and R. F. Werner, *Comm. Math. Phys.* **144**, 443–490 (1992).
  - [20] F. Verstraete and J. I. Cirac, *Phys. Rev. A* **70**, 060302 (2004).
  - [21] D. Perez-Garcia, F. Verstraete, M. M. Wolf, and J.I. Cirac, *Quant. Inf. Comp.* **7**, 401 (2007).
  - [22] T.-C. Wei et al., *Phys. Rev. A* **67**, 022110 (2003).
  - [23] N. Gisin and S. Massar, *Phys. Rev. Lett.* **79**, 2153 (1997).
  - [24] M. Mohseni et al., *Phys. Rev. Lett.* **91**, 187903 (2003).
  - [25] Tame et al., *Phys. Rev. Lett.* **98**, 140501 (2007).
  - [26] D. Deutsch and R. Jozsa, *Proc. R. Soc. A* **439**, 553 (1992).
  - [27] M. Varnava, D. E. Browne, T. Rudolph, *Phys. Rev. Lett.* **100**, 060502 (2008).
  - [28] D. Gross, K. Kieling, and J. Eisert, *Phys. Rev. A* **74**, 042343 (2006).
  - [29] P. G. Kwiat et al. *Phys. Rev. Lett.* **75**, 4337 (1995).
  - [30] N. Kiesel et al., *Phys. Rev. Lett.* **95**, 210505 (2005).
  - [31] W.-B. Gao et al., arXiv: quant-ph/08094277.

**APPENDIX: EXPERIMENTAL DEMONSTRATION OF MEASUREMENT-BASED QUANTUM COMPUTATION IN CORRELATION SPACE**

**Universal scheme for coupling 1D computational wires into a 2D resource**

The scheme we demonstrate in our experiment to couple two 1D computational wires and the measurement pattern for the implementation of an entangling gate is rather general and applicable to arbitrary computational wires. In the following, we reformulate the scheme for general wires, which our experiment provides a specific example of.

Quantum wires, with tensor matrices in the canonical form [1] as  $A[|0\rangle] = W$  and  $A[|1\rangle] = WS(\theta)$  where  $S(\theta) = \text{diag}(e^{-i\frac{\theta}{2}}, e^{i\frac{\theta}{2}})$ , can be coupled into a 2D resource state which is universal for measurement based quantum computation. The coupling scheme used in the experiment is depicted in Fig. 1. Qubit 4 is first prepared in  $|+\rangle = 2^{-1/2}(|0\rangle + |1\rangle)$ , two controlled-X gates (in the same basis as the canonical form of the tensor matrices) are applied between qubits 2 and 4, qubits 4 and 6. The scheme is universal in the sense that it works for all general wires in the canonical form and the applied coupling gates, namely controlled-X gates, are independent of the specific quantum wire. To decouple the wires, we only need to measure qubit 4 in the computational basis  $\{|0\rangle, |1\rangle\}$ . If the outcome is 0, we have un-done the coupling; otherwise we get the original 1D wires, up to the action of  $\sigma_x$  on qubits 2 and 6.

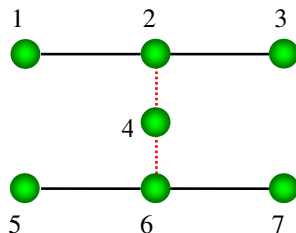


FIG. 1: (Color online) Universal coupling scheme for arbitrary quantum wires. Qubit 4 is first prepared in the state  $|+\rangle$ , two controlled-X gates (in the basis of the canonical form of the tensor matrices) are applied between qubits 2 and 4, qubits 4 and 6 (red dashed lines).

To perform an entangling gate, we do the following measurements: (a) Measure qubits 2 and 6 in the basis  $\{u_0|0\rangle - u_1|1\rangle, u_1|0\rangle + u_0|1\rangle\}$ , where  $u_0 = 2^{-1/2}(\cos\frac{\theta}{4} - \sin\frac{\theta}{4})$  and  $u_1 = 2^{-1/2}(\cos\frac{\theta}{4} + \sin\frac{\theta}{4})$ , the outcomes are denoted as  $s_2$  and  $s_6$ ; (b) If  $s_2 = 1$  or  $s_6 = 1$ , measurement of qubit 4 in the computational basis will decouple the two quantum wires and the logical qubits, carried by the correlation systems corresponding to the two quantum wires, leaving a byproduct operator  $\mathcal{O}_b$ . We can then restart the procedure after compensating  $\mathcal{O}_b$  via the trial-until-success strategy [2, 3]; (c) If  $s_2 = s_6 = 0$ , we measure qubit 4 in the Y basis  $\{|0\rangle + i|1\rangle, |0\rangle - i|1\rangle\}$  and implement the controlled phase gate with a by-product operator  $[WS(\frac{\theta}{2}) \otimes WS(\frac{\theta}{2})] \cdot (\sigma_z \otimes \sigma_z)^{s_4} \cdot (I \otimes |0\rangle\langle 0| + \sigma_z \otimes |1\rangle\langle 1|)$  on the correlation systems. The trial-until-success strategy to compensate the randomness of measurement is used to guarantee the computational efficiency [2, 3] when we obtain the wrong measurement outcome in the above protocol.



### The characterization of the four-qubit state

To characterize the four-qubit state, we extracted its density matrix by the method of over-complete state tomography. We collected experimental data for 300s for each of the 1296 combinations of the measurement bases  $\{|H\rangle, |V\rangle, |P\rangle, |M\rangle, |R\rangle, |L\rangle\}$ , where  $|R\rangle = \frac{1}{\sqrt{2}}(|H\rangle + i|V\rangle)$  and  $|L\rangle = \frac{1}{\sqrt{2}}(|H\rangle - i|V\rangle)$ . With these data, the maximum-likelihood technique is used to construct the density matrix of the state. Even though the state may look different in Fig. 2, what is essential is the fidelity which characterizes how well the task is performed,  $F = \langle \psi_4 | \rho | \psi_4 \rangle = 0.74 \pm 0.01$ . Similar to the method in refs. [4, 5], the error bar of the fidelity is calculated by performing a 100 run Monte Carlo simulation of the whole state tomography analysis, with Poissonian noise added to each experimental data point in each run.

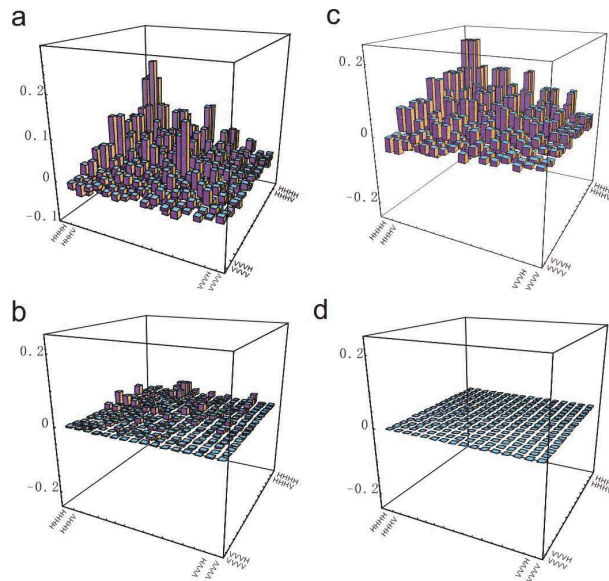


FIG. 2: **a.** The real parts of the measured four-qubit state density matrix. **b.** The real parts of the expected density matrix. **c.** The imaginary parts of the measured four-qubit density matrix. **d.** The imaginary parts of the expected density matrix.

### The fidelity of the six-qubit state

To obtain the fidelity of the six-qubit state  $|\psi_6\rangle$ , we use a method similar to using an entanglement witness [6, 7]. We decompose the density matrix  $|\psi_6\rangle\langle\psi_6|$  into locally measurable observables, the values of which can be obtained by measuring 36 settings. The qubit is carried by the polarization or path degree of freedom of a photon, i.e.  $|0\rangle \leftrightarrow |H\rangle, |H'\rangle$  and  $|1\rangle \leftrightarrow |V\rangle, |V'\rangle$ . The state  $|\psi_6\rangle$  can be given as

$$|\psi_6\rangle = \frac{1}{\sqrt{2}}(|a\rangle + |b\rangle) \quad (11)$$

where

$$\begin{aligned} |a\rangle &= |0\rangle_4 (c|00\rangle + s|11\rangle)_{33'} \otimes [c|0\rangle_2 (c|00\rangle + s|11\rangle)_{11'} + s|1\rangle_2 (c|00\rangle - s|11\rangle)_{11'}]; \\ |b\rangle &= |1\rangle_4 (c|00\rangle - s|11\rangle)_{33'} \otimes [c|0\rangle_2 (c|00\rangle + s|11\rangle)_{11'} - s|1\rangle_2 (c|00\rangle - s|11\rangle)_{11'}]. \end{aligned} \quad (12)$$

The decomposition of  $|\psi_6\rangle$  is

$$|\psi_6\rangle\langle\psi_6| = \sum_{i=0}^{36} M_i, \quad (13)$$

where

$$M_1 = I_4 \otimes (c^2 |00\rangle_{33'} \langle 00| + s^2 |11\rangle_{33'} \langle 11|) \otimes (c^2 |0\rangle_2 \langle 0| + s^2 |1\rangle_2 \langle 1|) \otimes (c^2 |00\rangle_{11'} \langle 00| + s^2 |11\rangle_{11'} \langle 11|); \quad (14)$$

$$M_2 = Z_4 \otimes (c^2 |00\rangle_{33'} \langle 00| + s^2 |11\rangle_{33'} \langle 11|) \otimes csX_2 \otimes (c^2 |00\rangle_{11'} \langle 00| + s^2 |11\rangle_{11'} \langle 11|); \quad (15)$$

$$M_3 = Z_4 \otimes \left( \frac{1}{2} csX_3 \otimes X_{3'} \right) \otimes (c^2 |0\rangle_2 \langle 0| + s^2 |1\rangle_2 \langle 1|) \otimes (c^2 |00\rangle_{11'} \langle 00| + s^2 |11\rangle_{11'} \langle 11|); \quad (16)$$

$$M_4 = I_4 \otimes (c^2 |00\rangle_{33'} \langle 00| + s^2 |11\rangle_{33'} \langle 11|) \otimes (s^2 |1\rangle_2 \langle 1| - c^2 |0\rangle_2 \langle 0|) \otimes \frac{1}{2} csY_1 \otimes Y_{1'}; \quad (17)$$

$$M_5 = I_4 \otimes (c^2 |00\rangle_{33'} \langle 00| + s^2 |11\rangle_{33'} \langle 11|) \otimes (c^2 |0\rangle_2 \langle 0| - s^2 |1\rangle_2 \langle 1|) \otimes \frac{1}{2} csX_1 \otimes X_{1'}; \quad (18)$$

$$M_6 = -Z_4 \otimes \left( \frac{1}{2} csY_3 \otimes Y_{3'} \right) \otimes (c^2 |0\rangle_2 \langle 0| + s^2 |1\rangle_2 \langle 1|) \otimes (c^2 |00\rangle_{11'} \langle 00| + s^2 |11\rangle_{11'} \langle 11|); \quad (19)$$

$$M_7 = I_4 \otimes \left( \frac{1}{2} csX_3 \otimes X_{3'} \right) \otimes csX_2 \otimes (c^2 |00\rangle_{11'} \langle 00| - s^2 |11\rangle_{11'} \langle 11|); \quad (20)$$

$$M_8 = I_4 \otimes \left( \frac{1}{2} csY_3 \otimes Y_{3'} \right) \otimes csX_2 \otimes (c^2 |00\rangle_{11'} \langle 00| - s^2 |11\rangle_{11'} \langle 11|); \quad (21)$$

$$M_9 = Z_4 \otimes (c^2 |00\rangle_{33'} \langle 00| + s^2 |11\rangle_{33'} \langle 11|) \otimes \frac{1}{2} c^2 s^2 Y_2 \otimes X_1 \otimes Y_{1'}; \quad (22)$$

$$M_{10} = Z_4 \otimes (c^2 |00\rangle_{33'} \langle 00| + s^2 |11\rangle_{33'} \langle 11|) \otimes \frac{1}{2} c^2 s^2 Y_2 \otimes Y_1 \otimes X_{1'}; \quad (23)$$

$$M_{11} = Z_4 \otimes \left( \frac{1}{2} csX_3 \otimes X_{3'} \right) \otimes (c^2 |0\rangle_2 \langle 0| - s^2 |1\rangle_2 \langle 1|) \otimes \frac{1}{2} csX_1 \otimes X_{1'}; \quad (24)$$

$$M_{12} = Z_4 \otimes \left( \frac{1}{2} csY_3 \otimes Y_{3'} \right) \otimes (s^2 |1\rangle_2 \langle 1| - c^2 |0\rangle_2 \langle 0|) \otimes \frac{1}{2} csX_1 \otimes X_{1'}; \quad (25)$$

$$M_{13} = Z_4 \otimes \left( \frac{1}{2} csX_3 \otimes X_{3'} \right) \otimes (s^2 |1\rangle_2 \langle 1| - c^2 |0\rangle_2 \langle 0|) \otimes \frac{1}{2} csY_1 \otimes Y_{1'}; \quad (26)$$

$$M_{14} = Z_4 \otimes \left( \frac{1}{2} csY_3 \otimes Y_{3'} \right) \otimes (c^2 |0\rangle_2 \langle 0| - s^2 |1\rangle_2 \langle 1|) \otimes \frac{1}{2} csY_1 \otimes Y_{1'}; \quad (27)$$

$$M_{15} = I_4 \otimes \left( \frac{1}{2} csX_3 \otimes X_{3'} \right) \otimes \frac{1}{2} c^2 s^2 Y_2 \otimes X_1 \otimes Y_{1'}; \quad (28)$$

$$M_{16} = I_4 \otimes \left( \frac{1}{2} csY_3 \otimes Y_{3'} \right) \otimes \frac{1}{2} c^2 s^2 Y_2 \otimes X_1 \otimes Y_{1'}; \quad (29)$$

$$M_{17} = I_4 \otimes \left( \frac{1}{2} csX_3 \otimes X_{3'} \right) \otimes \frac{1}{2} c^2 s^2 Y_2 \otimes Y_1 \otimes X_{1'}; \quad (30)$$

$$M_{18} = I_4 \otimes \left( \frac{1}{2} csY_3 \otimes Y_{3'} \right) \otimes \frac{1}{2} c^2 s^2 Y_2 \otimes Y_1 \otimes X_{1'}; \quad (31)$$

$$M_{19} = X_4 \otimes (c^2 |00\rangle_{33'} \langle 00| - s^2 |11\rangle_{33'} \langle 11|) \otimes (c^2 |0\rangle_2 \langle 0| - s^2 |1\rangle_2 \langle 1|) \otimes (c^2 |00\rangle_{11'} \langle 00| + s^2 |11\rangle_{11'} \langle 11|); \quad (32)$$

$$M_{20} = Y_4 \otimes (c^2 |00\rangle_{33'} \langle 00| - s^2 |11\rangle_{33'} \langle 11|) \otimes csY_2 \otimes (c^2 |00\rangle_{11'} \langle 00| - s^2 |11\rangle_{11'} \langle 11|); \quad (33)$$

$$M_{21} = X_4 \otimes (c^2 |00\rangle_{33'} \langle 00| - s^2 |11\rangle_{33'} \langle 11|) \otimes (c^2 |0\rangle_2 \langle 0| + s^2 |1\rangle_2 \langle 1|) \otimes \frac{1}{2} csX_1 \otimes X_{1'}; \quad (34)$$

$$M_{22} = X_4 \otimes (c^2 |00\rangle_{33'} \langle 00| - s^2 |11\rangle_{33'} \langle 11|) \otimes (c^2 |0\rangle_2 \langle 0| + s^2 |1\rangle_2 \langle 1|) \otimes \frac{1}{2} csY_1 \otimes Y_{1'}; \quad (35)$$

$$M_{23} = \frac{1}{2} csY_4 \otimes X_3 \otimes Y_{3'} \otimes (c^2 |0\rangle_2 \langle 0| - s^2 |1\rangle_2 \langle 1|) \otimes (c^2 |00\rangle_{11'} \langle 00| + s^2 |11\rangle_{11'} \langle 11|); \quad (36)$$

$$M_{24} = \frac{1}{2} csY_4 \otimes Y_3 \otimes X_{3'} \otimes (c^2 |0\rangle_2 \langle 0| - s^2 |1\rangle_2 \langle 1|) \otimes (c^2 |00\rangle_{11'} \langle 00| + s^2 |11\rangle_{11'} \langle 11|); \quad (37)$$

$$M_{25} = Y_4 \otimes (s^2 |11\rangle_{33'} \langle 11| - c^2 |00\rangle_{33'} \langle 00|) \otimes \frac{1}{2} c^2 s^2 X_2 \otimes X_1 \otimes Y_{1'}; \quad (38)$$

$$M_{26} = Y_4 \otimes (s^2 |11\rangle_{33'} \langle 11| - c^2 |00\rangle_{33'} \langle 00|) \otimes \frac{1}{2} c^2 s^2 X_2 \otimes Y_1 \otimes X_{1'}; \quad (39)$$

$$M_{27} = \frac{1}{2} cs X_4 \otimes X_3 \otimes Y_{3'} \otimes cs Y_2 \otimes (s^2 |11\rangle_{11'} \langle 11| - c^2 |00\rangle_{11'} \langle 00|); \quad (40)$$

$$M_{28} = \frac{1}{2} cs X_4 \otimes Y_3 \otimes X_{3'} \otimes cs Y_2 \otimes (s^2 |11\rangle_{11'} \langle 11| - c^2 |00\rangle_{11'} \langle 00|); \quad (41)$$

$$M_{29} = \frac{1}{2} cs Y_4 \otimes Y_3 \otimes X_{3'} \otimes (s^2 |1\rangle_2 \langle 1| - c^2 |0\rangle_2 \langle 0|) \otimes \frac{1}{2} cs Y_1 \otimes Y_{1'}; \quad (42)$$

$$M_{30} = \frac{1}{2} cs Y_4 \otimes Y_3 \otimes X_{3'} \otimes (c^2 |0\rangle_2 \langle 0| - s^2 |1\rangle_2 \langle 1|) \otimes \frac{1}{2} cs X_1 \otimes X_{1'}; \quad (43)$$

$$M_{31} = \frac{1}{2} cs Y_4 \otimes X_3 \otimes Y_{3'} \otimes (c^2 |0\rangle_2 \langle 0| - s^2 |1\rangle_2 \langle 1|) \otimes \frac{1}{2} cs X_1 \otimes X_{1'}; \quad (44)$$

$$M_{32} = \frac{1}{2} cs Y_4 \otimes X_3 \otimes Y_{3'} \otimes (s^2 |1\rangle_2 \langle 1| - c^2 |0\rangle_2 \langle 0|) \otimes \frac{1}{2} cs Y_1 \otimes Y_{1'}; \quad (45)$$

$$M_{33} = \frac{1}{2} cs X_4 \otimes Y_3 \otimes X_{3'} \otimes \frac{1}{2} c^2 s^2 X_2 \otimes X_1 \otimes Y_{1'}; \quad (46)$$

$$M_{34} = \frac{1}{2} cs X_4 \otimes Y_3 \otimes X_{3'} \otimes \frac{1}{2} c^2 s^2 X_2 \otimes Y_1 \otimes X_{1'}; \quad (47)$$

$$M_{35} = \frac{1}{2} cs X_4 \otimes X_3 \otimes Y_{3'} \otimes \frac{1}{2} c^2 s^2 X_2 \otimes X_1 \otimes Y_{1'}; \quad (48)$$

$$M_{36} = \frac{1}{2} cs X_4 \otimes X_3 \otimes Y_{3'} \otimes \frac{1}{2} c^2 s^2 X_2 \otimes Y_1 \otimes X_{1'}. \quad (49)$$

To obtain the experimental values of the above operators, we need to measure using the 36 measurement settings (4-3-3'-2-1-1'): ZZZZZZ; ZXXZZZ; ZYYZZZ; ZZZZXX; ZXXZXX; ZYYZXX; ZZZZYY; ZXXZY; ZYYZY; ZZZXZZ; ZXXXZZ; ZYXXZZ; ZZZYXY; ZXXYXY; ZYYYXY; ZZZYYX; ZXXYYX; ZYYYYX; XZZZZZ; XZZZXX; XZZZYY; XYXYZZ; XYXXXY; XYZZYX; XYYZZZ; XXYXXY; XXYXYX; YYXZZZ; YYXZXX; YYXZYY; YXYZZZ; YXYZXX; YXYZYY; YZZYZZ; YZZXXY; YZZXYX. The theoretical and experimental values of the 36 observables are listed in Fig. 3.

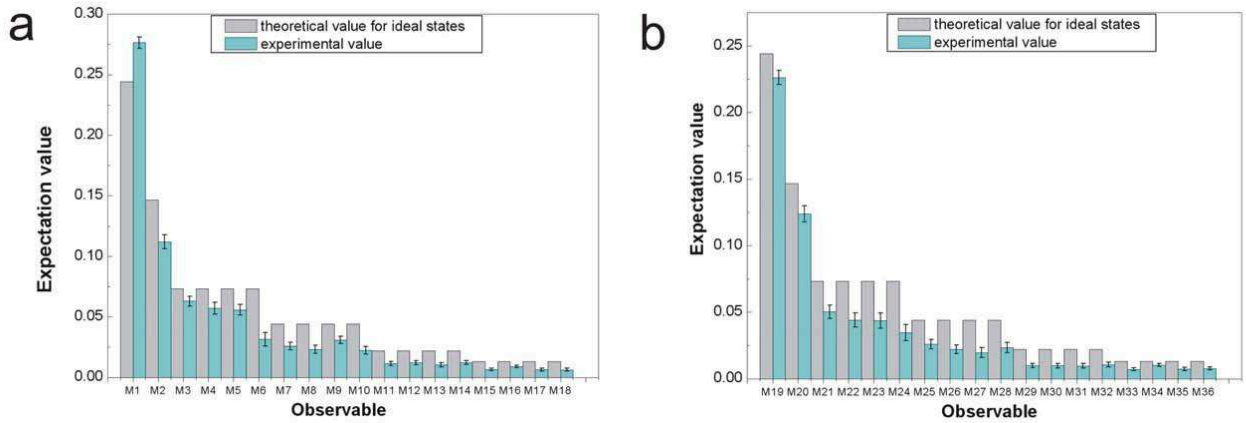


FIG. 3: The theoretical and experimental values of the required 36 observables. **a**, The required 18 observables to obtain the value of  $|a\rangle\langle a| + |b\rangle\langle b|$ ; **b**, the required 18 observables to obtain the value of  $|a\rangle\langle b| + |b\rangle\langle a|$ , where  $|a\rangle$  and  $|b\rangle$  are states in Eq. (2).

### Additional experimental results of the single-qubit gate

Based on the generated four-qubit state, an arbitrary SU(2) single-qubit rotation can be implemented by the consecutive measurements  $B_1(\alpha)$ ,  $B_2(\beta)$ ,  $B_3(\gamma)$  on the physical qubits 1, 2, 3, transforming the correlation system from the state  $|\psi_{in}\rangle_c = |+\rangle$  to  $|\psi_{out}\rangle_c = \hat{H}R_z(\gamma)R_x(\beta)R_z(\alpha)|+\rangle$ , with the corresponding physical output state being  $|\psi_{out}\rangle_p = R_z(\gamma)R_x(\beta)R_z(\alpha)|+\rangle|_{0 \rightarrow H,1 \rightarrow V}$ . In Table I, we give additional experimental results of the fidelities of the output states.

$\alpha$	$\beta$	$\gamma$	$ \psi_{out}\rangle_c$	$ \psi_{out}\rangle_p$	fidelity
$\pi$	0	$\pi/3$	$\frac{1}{2} 0\rangle + \frac{\sqrt{3}i}{2} 1\rangle$	$\frac{1}{2} P\rangle + \frac{\sqrt{3}i}{2} M\rangle$	$0.78 \pm 0.01$
0	0	$-\pi/3$	$\frac{\sqrt{3}}{2} 0\rangle + \frac{i}{2} 1\rangle$	$\frac{\sqrt{3}}{2} P\rangle + \frac{i}{2} M\rangle$	$0.88 \pm 0.01$
$\pi/2$	$2\pi/3$	$\pi/2$	$\frac{\sqrt{3}}{2} 0\rangle + \frac{1}{2} 1\rangle$	$\frac{\sqrt{3}}{2} P\rangle + \frac{1}{2} M\rangle$	$0.91 \pm 0.02$
$\pi/2$	$\pi/3$	$\pi/2$	$\frac{1}{2} 0\rangle + \frac{\sqrt{3}}{2} 1\rangle$	$\frac{1}{2} P\rangle + \frac{\sqrt{3}}{2} M\rangle$	$0.84 \pm 0.02$
$\pi/2$	$2\pi/3$	0	$\frac{1}{2} -\rangle - \frac{\sqrt{3}i}{2} +\rangle$	$\frac{1}{2} V\rangle - \frac{\sqrt{3}i}{2} H\rangle$	$0.70 \pm 0.02$
$\pi/2$	$\pi/3$	0	$\frac{\sqrt{3}}{2} -\rangle - \frac{i}{2} +\rangle$	$\frac{\sqrt{3}}{2} V\rangle - \frac{i}{2} H\rangle$	$0.74 \pm 0.02$

TABLE II: The fidelities of the output states of the single-qubit rotation. The first three qubits of the four-qubit cluster state are respectively measured in bases  $B(\alpha)$ ,  $B(\beta)$ ,  $B(\gamma)$ .  $|\psi_{out}\rangle_c$  and  $|\psi_{out}\rangle_p$  represent the output states in the correlation space and the physical world, respectively. In each case, the fidelity is achieved by measuring in 20 minutes.

### Trial-until-success strategy to compensate the randomness of measurement outcome

The implementation of an arbitrary SU(2) single-qubit rotation can be achieved by measuring the qubits, with the tensor matrices  $A[|H\rangle] = \hat{H} \cos \theta$  and  $A[|V\rangle] = \hat{H} \hat{Z} \sin \theta$ , in the following basis  $B(\alpha) = \{|\alpha_0\rangle, |\alpha_1\rangle\}$ , where  $|\alpha_0\rangle = \sin \theta |H\rangle + i \cos \theta \tan \frac{\alpha}{2} |V\rangle$  and  $|\alpha_1\rangle = \cos \theta |H\rangle - i \sin \theta \cot \frac{\alpha}{2} |V\rangle$ . If the outcome  $r = 0$ , we realize the desired operation  $\hat{H}R_z(\alpha)$  with the success probability as

$$p_s(\alpha) = \frac{\sin^2 2\theta}{2(1 - \cos 2\theta \cos \alpha)} \geq \frac{\sin^2 2\theta}{2(1 + |\cos 2\theta|)} \equiv p_\theta \quad (50)$$

Thus, once  $\sin(2\theta) \neq 0$ , the success probability  $p_s(\alpha)$  is always lower bounded by a positive constant (i.e. independent on the angle  $\alpha$ ). If we get the wrong outcome  $r = 1$ , with the probability  $1 - p_s(\alpha)$ , we actually implement an operation  $\hat{H}R_z(\alpha')$  with the wrong angle  $\tan(\alpha'/2) = (-1/3) * \cot(\alpha/2)$ . To compensate this error, we measure the first qubit in the Z basis  $\{|H\rangle, |V\rangle\}$  obtaining outcome  $r_1$  and the second qubit in the basis  $B[(-1)^{r_1}(\alpha - \alpha')]$  with outcome  $r_2$ . When  $r_2 = 0$ , which occurs with probability  $p_s(\alpha - \alpha')$ , we obtain the desired rotation  $\hat{H}R_z(\alpha)$  up to a Pauli by-product operator. Thus, with such a block of two more qubits, we can boost the success probability of the rotation from  $p_s(\alpha)$  to  $p_s(\alpha) + [1 - p_s(\alpha)] \cdot p_s(\alpha - \alpha')$ . In the experiment, we have demonstrated such a building block to compensate the unwanted by-product operators induced by the wrong measurement outcome. In principle, one can generalize this technique to achieve a success probability arbitrary close to 1. Assume we have  $n$  blocks, the success probability will be lower bounded by  $p_s(\alpha) + [1 - p_s(\alpha)][1 - (1 - p_\theta)^n]$  by repeating the above procedure. It can be verified that, for arbitrary  $\epsilon > 0$ , the extra computational overhead (the number of qubits) needed to achieve a success probability higher than  $1 - \epsilon$  scales polynomially as  $O(\log \frac{1}{\epsilon})$ . The same analysis is valid also for the implementation of two-qubit entangling gates when we get the wrong measurement outcomes. Therefore, our experiment realizes a proof-of-principle demonstration of the trial-until-success strategy to compensate the randomness of the measurement outcomes in measurement-based quantum computation with non-cluster states.

### Additional experimental results of the two-qubit entangling gate

In the experiment of the two-qubit entangling gate, when  $r_2 = r_3 = 0$ , we use state tomography to characterize the output two-qubit state of the two-qubit gate. In Fig. 4, we list the experimental and theoretical density matrices when  $r_4 = 1$ ,  $\alpha = 0$  and  $r_4 = 1$ ,  $\alpha = \pi/3$ . Also, we give the results when  $\alpha$  takes the value of  $\pi$  or  $\pi/2$ .

When  $r_2 \neq 0$  or  $r_3 \neq 0$ , we measurement qubit 4 in the Z basis  $\{|H\rangle, |V\rangle\}$  and decouple the two quantum wires. Rotation errors will be introduced in the operation, which can be compensated via the trial-until-success strategy as

demonstrated above. We have measured the fidelities of the experimental states and compare them with the expected ones, the results of which are listed in Table II when  $\alpha$  is set to one of the angles  $\{0, \pi, \pi/2, \pi/3\}$ .

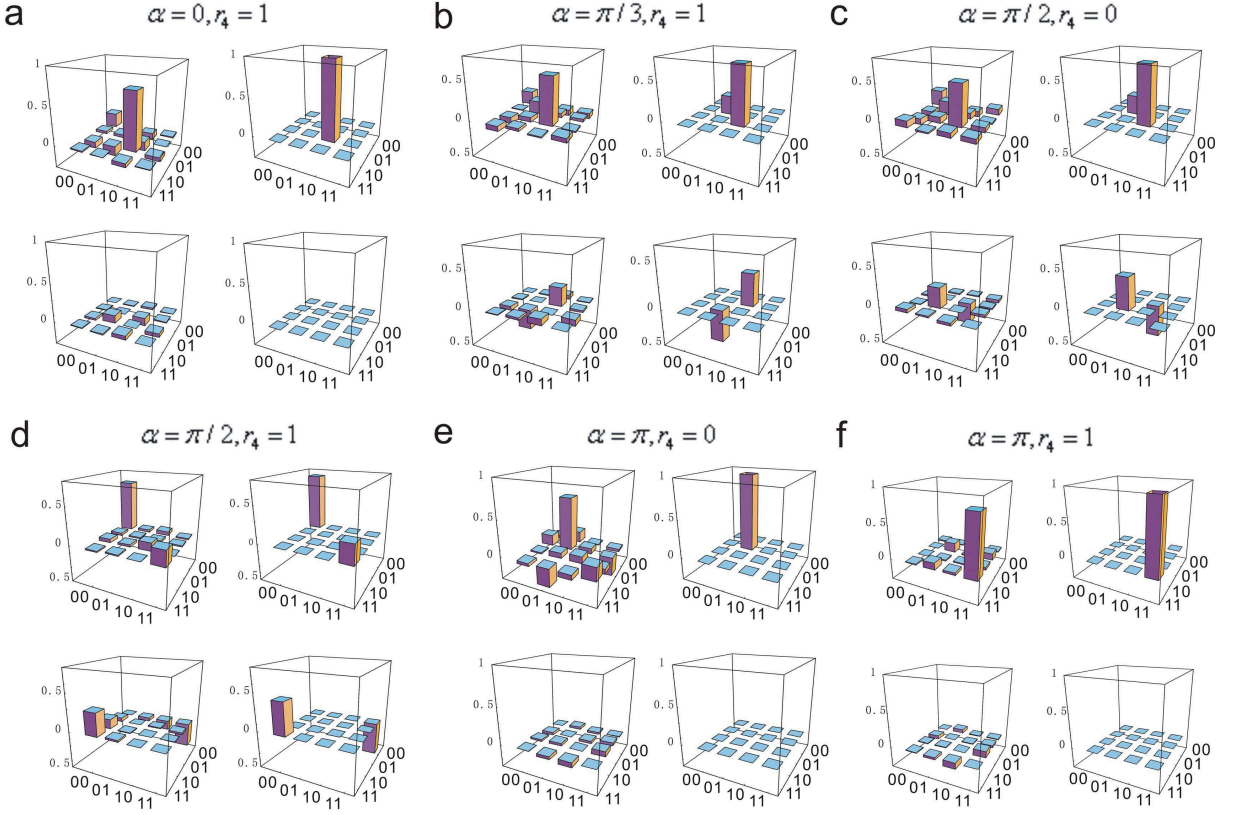


FIG. 4: The density matrices of the output states of the entangling two-qubit gate. In each sub-fig, the left-top: the real part of the experimental density matrices; the right-top: the real part of the expected density matrix; the left-bottom: the imaginary part of the experimental density matrices; the right-bottom: the imaginary part of the expected density matrix. The fidelity of each state is: **a**:  $0.80 \pm 0.03$ ; **b**:  $0.76 \pm 0.04$ ; **c**:  $0.79 \pm 0.03$ ; **d**:  $0.74 \pm 0.04$ ; **e**:  $0.75 \pm 0.02$ ; **f**:  $0.86 \pm 0.02$ .

## DEUTSCH'S ALGORITHM

In the main text, we consider only the case of  $r_1 = r_2 = r_3 = r_4 = 0$ . Here we discuss in detail the cases when one or more outcome of four measurements is not 0.

First, let us consider the implementation of the balanced function. We know that if we measure qubit 1 in the basis  $B(\pi)$  and qubits 2, 3, 4 in the basis  $B(\pi/2)$ , balanced function can be implemented with the outcome  $r_1 = r_2 = r_3 = r_4 = 0$ . Below we discuss another two situations. (a) When  $r_2 = r_3 = 0$  & ( $r_1 \neq 0$  or  $r_4 \neq 0$ ), Pauli errors may occur on the output states, which will change the distribution of the final results. However, we can classically relabel the results to correct errors of the distribution. With regards to the classical relabeling, the detector signal corresponding to  $r_2 = r_3 = 0$ , together with the measurements of the qubits 2, 3, 4 should be viewed as the entire function in the black box. In this case, the experimental results are shown in Fig. 5a and the probability of successfully judging the types of the functions is  $82\% \pm 3\%$ . (b) When  $r_2 \neq 0$  or  $r_3 \neq 0$ , we can't implement the entangling gate with the given qubits and thus can't implement the balanced function.

Next, we consider the case of implementing the constant function. When qubit 1 is measured in the basis  $B(\pi)$  and qubits 2, 3, 4 in the basis  $B(0)$ , we can simulate the constant function with the outcome  $r_1 = r_2 = r_3 = r_4 = 0$ . However, when the measurements are not zero, Pauli errors may occur on the output states and change the distribution. As with the implementation of the balanced function, we can also relabel the results. Considering again the case with the measurement results  $r_2 = r_3 = 0$ , in Fig. 5b we show the experimental data when  $r_1$  and  $r_4$  take the value of either 0 or 1. The success probability of recognizing the constant function is as large as  $99\% \pm 1\%$ .

$\alpha$	$r_2$	$r_3$	$r_4$	the expected physical state	fidelity	$\alpha$	$r_2$	$r_3$	$r_4$	the expected physical state	fidelity
0	0	1	0	$ 0\rangle_{1'} (\frac{3}{\sqrt{10}} 0\rangle + \frac{i}{\sqrt{10}} 1\rangle)_{3'}$	$0.96 \pm 0.02$	0	1	0	0	$ 0\rangle_{1'}  L\rangle_{3'}$	$0.91 \pm 0.02$
0	0	1	1	$ 0\rangle_{1'} (\frac{3}{\sqrt{10}} 0\rangle - \frac{i}{\sqrt{10}} 1\rangle)_{3'}$	$0.95 \pm 0.02$	0	1	0	1	$ 0\rangle_{1'}  R\rangle_{3'}$	$0.86 \pm 0.02$
$\pi$	0	1	0	$ 1\rangle_{1'} (\frac{3}{\sqrt{10}} 0\rangle + \frac{i}{\sqrt{10}} 1\rangle)_{3'}$	$0.97 \pm 0.03$	$\pi$	1	0	0	$ 1\rangle_{1'}  L\rangle_{3'}$	$0.88 \pm 0.02$
$\pi$	0	1	1	$ 1\rangle_{1'} (\frac{3}{\sqrt{10}} 0\rangle - \frac{i}{\sqrt{10}} 1\rangle)_{3'}$	$0.88 \pm 0.03$	$\pi$	1	0	1	$ 1\rangle_{1'}  R\rangle_{3'}$	$0.89 \pm 0.02$
$\pi/2$	0	1	0	$ +\rangle_{1'} (\frac{3}{\sqrt{10}} 0\rangle + \frac{i}{\sqrt{10}} 1\rangle)_{3'}$	$0.88 \pm 0.03$	$\pi/2$	1	0	0	$\frac{\sqrt{2}}{2}( 0\rangle - \frac{3+4i}{5} 1\rangle)_{1'}  L\rangle_{3'}$	$0.81 \pm 0.02$
$\pi/2$	0	1	1	$ -\rangle_{1'} (\frac{3}{\sqrt{10}} 0\rangle - \frac{i}{\sqrt{10}} 1\rangle)_{3'}$	$0.80 \pm 0.03$	$\pi/2$	1	0	1	$\frac{\sqrt{2}}{2}( 0\rangle + \frac{3-4i}{5} 1\rangle)_{1'}  R\rangle_{3'}$	$0.80 \pm 0.02$
$\pi/3$	0	1	0	$(\frac{\sqrt{3}}{2} 0\rangle + \frac{1}{2} 1\rangle)_{1'} (\frac{3}{\sqrt{10}} 0\rangle + \frac{i}{\sqrt{10}} 1\rangle)_{3'}$	$0.94 \pm 0.03$	$\pi/3$	1	0	0	$(\frac{\sqrt{3}}{2} 0\rangle - \frac{3+4i}{10} 1\rangle)_{1'}  L\rangle_{3'}$	$0.82 \pm 0.02$
$\pi/3$	0	1	1	$(\frac{\sqrt{3}}{2} 0\rangle - \frac{1}{2} 1\rangle)_{1'} (\frac{3}{\sqrt{10}} 0\rangle - \frac{i}{\sqrt{10}} 1\rangle)_{3'}$	$0.78 \pm 0.03$	$\pi/3$	1	0	1	$(\frac{\sqrt{3}}{2} 0\rangle + \frac{3-4i}{10} 1\rangle)_{1'}  R\rangle_{3'}$	$0.82 \pm 0.03$
0	1	1	0	$ 0\rangle_{1'} (\frac{3}{\sqrt{10}} 0\rangle + \frac{i}{\sqrt{10}} 1\rangle)_{3'}$	$0.99 \pm 0.02$	$\pi/2$	1	1	0	$(\frac{\sqrt{3}}{2} 0\rangle - \frac{3+4i}{10} 1\rangle)_{1'} (\frac{3}{\sqrt{10}} 0\rangle + \frac{i}{\sqrt{10}} 1\rangle)_{3'}$	$0.83 \pm 0.03$
0	1	1	1	$ 0\rangle_{1'} (\frac{3}{\sqrt{10}} 0\rangle - \frac{i}{\sqrt{10}} 1\rangle)_{3'}$	$0.96 \pm 0.02$	$\pi/2$	1	1	1	$\frac{\sqrt{2}}{2}( 0\rangle + \frac{3-4i}{5} 1\rangle)_{1'} (\frac{3}{\sqrt{10}} 0\rangle - \frac{i}{\sqrt{10}} 1\rangle)_{3'}$	$0.74 \pm 0.03$
$\pi$	1	1	0	$ 1\rangle_{1'} (\frac{3}{\sqrt{10}} 0\rangle + \frac{i}{\sqrt{10}} 1\rangle)_{3'}$	$0.96 \pm 0.03$	$\pi/3$	1	1	0	$(\frac{\sqrt{3}}{2} 0\rangle - \frac{3+4i}{10} 1\rangle)_{1'} (\frac{3}{\sqrt{10}} 0\rangle + \frac{i}{\sqrt{10}} 1\rangle)_{3'}$	$0.88 \pm 0.02$
$\pi$	1	1	1	$ 1\rangle_{1'} (\frac{3}{\sqrt{10}} 0\rangle - \frac{i}{\sqrt{10}} 1\rangle)_{3'}$	$0.88 \pm 0.03$	$\pi/3$	1	1	1	$(\frac{\sqrt{3}}{2} 0\rangle + \frac{3-4i}{10} 1\rangle)_{1'} (\frac{3}{\sqrt{10}} 0\rangle - \frac{i}{\sqrt{10}} 1\rangle)_{3'}$	$0.81 \pm 0.02$

TABLE III: The fidelities of the output states of the two-qubit entangling gate when we get the wrong measurement outcomes. We measure qubit 1 in the basis  $B_1(\alpha)$  to prepare the input logical state, and measure qubits 2, 3 and 4 in the bases  $B_2(\frac{\pi}{2}) = B_3(\frac{\pi}{2}) = \{s|H\rangle + ic|V\rangle, c|H\rangle - is|V\rangle\}$  and the Z basis  $\{|H\rangle, |V\rangle\}$  respectively. The measurement outcomes are  $r_2$ ,  $r_3$  and  $r_4$ . The path degree of freedom of a photon is denoted as  $H' \rightarrow 0$ ,  $V' \rightarrow 1$  in the physical states.

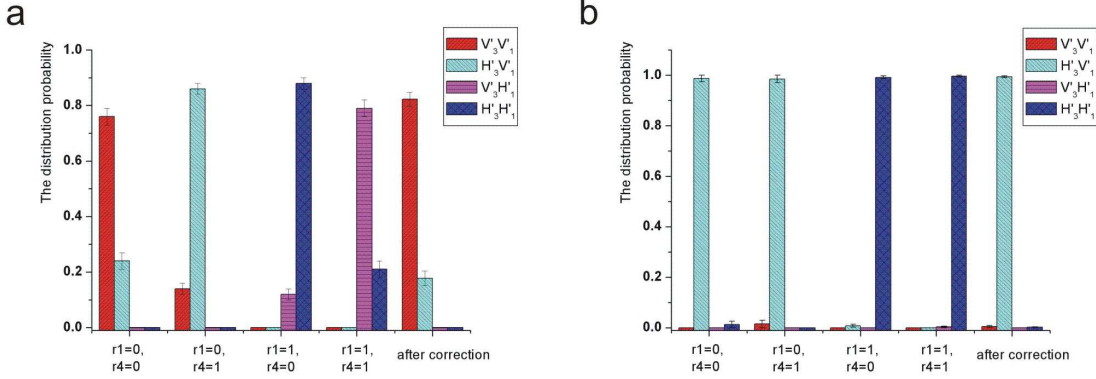


FIG. 5: **a.** The distribution of the final results when the function is balanced. The success probability of recognizing the constant function is  $82\% \pm 3\%$ . **b.** The distribution of the final results when the function is constant. The success probability of recognizing the constant function is  $99\% \pm 1\%$ .

- [1] D.Gross, J. Eisert, arXiv:0810.2542.
- [2] D.Gross, J. Eisert, *Phys. Rev. Lett.* **98**, 220503 (2007).
- [3] D. Gross, J. Eisert, N. Schuch, D. Perez-Garcia, *Phys. Rev. A* **76**, 052315 (2007).
- [4] M.S. Tame et al., *Phys. Rev. Lett.* **98**, 140501 (2007).
- [5] A.G. White et al., *Phys. Rev. Lett.* **83**, 3103 (1999); D. James et al., *Phys. Rev. A* **64**, 052312 (2001).
- [6] D. James, P.G. Kwiat, W. Munro, A. White, *Phys. Rev. A* **64**, 052312 (2001).
- [7] M. Bourennane, et al. *Phys. Rev. Lett.* **92**, 087902 (2003).